In vivo colonic epithelial cell editing attenuates intestinal inflammation in mice

[1,2,3,5]Hailing Zhang，[1,2,3,5]Hengxing Lu，[1,2,3,5]Shaolong Zhang，[1,2,3]Xukai Hu，[1,2,3]Qixing Wu, [1,2,3] Zi qin Yu，[2]Natasha Karyn Lienanto,[1,2,3,4] Jin Zhang

1. Center for Stem Cell and Regenerative Medicine, Department of Basic Medical Sciences, and Bone Marrow Transplantation Center of the First Affiliated Hospital, Zhejiang University School of Medicine, Hangzhou, China

2. Center for Stem Cell and Regenerative Medicine, Department of Basic Medical Sciences, Zhejiang University School of Medicine, Hangzhou, China

3. Liangzhu Laboratory, Zhejiang University, Hangzhou, China

4. Center of Gene and Cell Therapy and Genome Medicine of Zhejiang Province, Hangzhou, China

5. These authors contributed equally:

Abstract

Engineered epithelial cells with enhanced efferocytosis capacity promote inflammation resolution and restore tissue homeostasis. Here, we developed a therapeutic approach to generate efferocytosis boosting epithelial cells in vivo by delivering mRNA in lipid nanoparticles (LNPs). We demonstrate that LNP-mediated delivery of mRNA enables efficient in vitro and in vivo functional editing of epithelial cells. In murine models of colitis, intraperitoneal administration of mRNA-loaded nanoparticles designed to boost efferocytosis markedly attenuated intestinal inflammation and halted disease progression. This strategy provides a proof of concept that epithelial cells can be functional engineered in situ and represents a promising therapeutic avenue for mitigating inflammatory tissue damage.

Graphical Abstract

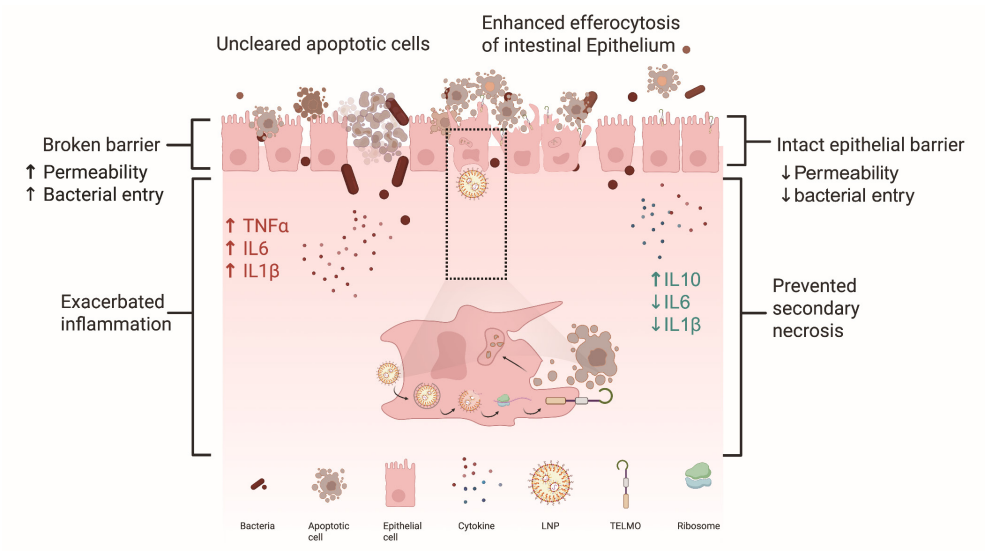

Introduction

Phagocytes mediate the rapid clearance of apoptotic cells in a process known as efferocytosis, which is critical for tissue homeostasis and inflammation resolution[1–6]. Inadequate efferocytosis has been associated with multiple inflammatory disorders, such as atherosclerosis, systemic lupus erythematosus (SLE) and inflammatory bowel disease (IBD), contributing to pathological inflammation and tissue damage[7–10]. Sophisticated studies in transgene-overexpressing mice have demonstrated that enhancing apoptotic cell clearance can be beneficial for resolution of inflammation[11–13]. In clinical practice, editing phagocytes in situ to prompt efferocytosis may offer new opportunities for treating these diseases. In this study, we explore the use of lipid-based nanoparticles (LNPs) to deliver a chimeric efferocytic receptor (TELMO)[12], with the goal of boosting efferocytosis as a therapeutic strategy against intestinal inflammation in mice. In a dextran sulfate sodium (DSS)-induced colitis model, intraperitoneal administration of LNPs preferentially targeted intestinal epithelial cells, resulting in robust TELMO expression and accelerated clearance of apoptotic corpses, which ultimately ameliorated inflammation and promoted tissue repair.

Results

We generated modified mRNA encoding an efferocytosis boosting chimeric receptor, termed TELMO, which was constructed by fusing the extracellular

phosphatidylserine recognition domains of TIM4 with the intracellular effector domain of ELMO1. To facilitate monitoring of TELMO expression, an enhanced green-fluorescent protein (EGFP) reporter was co-expressed via a 2A peptide (Fig. 1A). As shown in Fig. 1B and Fig. S1, the LNPs we produced demonstrated normal particle size and zeta potential values (Fig. 1B, S1). To determine whether the mRNA could be efficiently delivered into epithelial cells, we packaged the TELMO-2A-EGFP mRNA to LNPs and incubated them with HCT116 cells in vitro. Flow cytometry analysis demonstrated that LNPs were highly efficient in delivering mRNA to cultured epithelial cells, resulting in robust cell surface expression of TELMO in nearly all cells following transfection (Fig. 1C). To assess the ability of the LNP-editing cells to engulf apoptotic cells, we used staurosporine (STS)-treated Jurkat cells as apoptotic targets[14]. Successful induction of apoptosis was confirmed by Annexin V staining (Fig. S2A). The engulfment of CellTrace-labeled apoptotic cells by TELMO-expressing epithelial cells was progressively elevated over time, as shown by flow cytometry at multiple time points (Fig. 1D, Fig. S2B). This demonstrated that LNP-meditated TELMO expression significantly boosted apoptotic cell uptake. Confocal imaging also corroborated these findings, revealing more apoptotic cells localized around and within phagocytes (Fig. 1E). This observation suggests efficient internalization, prompting further investigation into the ensuing intracellular processing dynamics. To investigate the intracellular processing of apoptotic cells after TELMO-mediated efferocytosis,

77 we performed a corpse acidification assay using a dye-quenching approach
78 (Fig. 1F). TELMO expression significantly enhanced acidification, TELMO
79 expression significantly enhanced the acidification process, as shown by a
80 reduction in mean fluorescence intensity (MFI), indicating accelerated apoptotic
81 cargo processing (Fig. 1G, S3A). To further validate this observation, we utilized
82 a pH-sensitive reporter dye that fluoresces specifically in acidic compartments.
83 TELMO not only increased the percentage of phagocytes that trafficked
84 apoptotic corpses to acidic organelles (Fig. 1H, S3B), but also elevated the
85 acidified cargo intensity per cell (Fig. 1I, S3C). Additionally, confocal microscopy
86 confirmed that TELMO promotes both efficient internalization and processing
87 of apoptotic cells (Fig. 1J).

88 We next examined the ability of LNP mRNA to modify epithelial cells in vivo.
89 TELMO-EGFP-encoding LNPs were administered by intraperitoneal injection
90 in mice, and colon tissues were collected after 24 hours for analysis. EGFP
91 expression was observed in colonic epithelial cells by fluorescence microscopy,
92 indicating effective LNP-mediated delivery and functional expression of the
93 engineered constructs (Fig. 2A). Further flow cytometry analysis demonstrated
94 that TELMO was expressed in approximately 50% of EpCAM-positive cells,
95 thus confirming the highly efficient engineering of intestinal epithelium via LNP-
96 mediated mRNA delivery (Fig. 2B, S4). Encouraged by the efficient in vivo
97 engineering of colonic epithelial cells, we next evaluated the therapeutic
98 potential of TELMO mRNA delivery in a mouse model of colitis. TELMO-LNPs

99 or, as a control, GFP-LNPs were intraperitoneally (i.p.) injected into DSS-
100 exposed C57BL/6 mice according to the procedure outlined depicted in Figure
101 2C. The colitic mice received LNP treatments on days 0 and 3. Clinical signs of
102 colitis, including body weight change, stool consistency, and rectal bleeding,
103 were monitored daily. On day 10, colon length and histology were evaluated.
104 We found that TELMO-LNP treatment significantly mitigated the clinical
105 manifestations of DSS-induced colitis. Mice receiving TELMO-LNPs showed
106 significantly reduced disease severity, as evidenced by attenuated body weight
107 loss (Fig. S5A), improved stool consistency (Fig. S5B), and less rectal bleeding
108 (Fig. S5C), resulting in lower Disease Activity Index (DAI) scores (Fig. 2D and
109 S5D). Moreover, intestinal epithelial permeability was analyzed by FITC-
110 dextran leakage assay. The serum level of FITC-Dextran was significantly
111 increased in control mice, but this increase was markedly attenuated by
112 TELMO-LNP treatment (Fig. 2E). Consistent with the symptom improvement,
113 TELMO-LNPs also alleviated colon shortening (Fig. 2F, 2G), indicating reduced
114 tissue damage and inflammation at the gross anatomical level. This result
115 suggests that TELMO-LNPs helped restore intestinal barrier integrity, thereby
116 preventing bacterial translocation and subsequent systemic inflammation.
117 Corresponding to these functional improvements, histological examination also
118 confirmed preservation of tissue architecture at the microscopic level.
119 Compared to vehicle controls, TELMO-LNP-treated mice exhibited more intact
120 crypt structures, diminished mucosal erosion, and reduced inflammatory cell

infiltration (Fig. 2H, 2I). TUNEL staining further demonstrated minimal epithelial apoptotic cell death following TELMO-LNP treatment (Fig. 3A, 3B), suggesting that tissue integrity was preserved through active cytoprotection rather than merely delayed inflammatory damage. To evaluate the level of tissue inflammation, we performed qPCR analysis on colonic tissues. The results showed that the expression of pro-inflammatory cytokines (TNF-α, IL-1β, and IL-6) and chemokine-related genes (CXCL9 and CCL-2) was significantly downregulated in the treatment group. In contrast, the anti-inflammatory gene IL-10 was markedly upregulated (Fig. 3C-3H). Collectively, these results suggest that in vivo editing of colonic epithelial cells via TELMO-LNPs not only ameliorates clinical symptoms and preserves tissue architecture, but also reshapes the inflammatory microenvironment toward a more anti-inflammatory state.

Discussion

Gut inflammatory disorders, such as ulcerative colitis (UC) and IBD affect millions of people worldwide. Conventional therapeutic approaches are primarily ameliorative and often fail to address the underlying etiology of these diseases[15]. Colonic epithelial cells constitute the physical barrier and are fundamentally required for maintaining its integrity. Their role in clearing apoptotic neighbors is critical for the resolution of intestinal inflammation[11,16]. The rapid, potent, and transient expression of mRNA-encoded proteins, which

avoids the risk of detrimental genomic integration, makes them an attractive therapeutic platform[17]. In recent years, in vitro transcribed mRNA has shown promise for treating a broad spectrum of diseases, including cancer, fibrosis, and autoimmune diseases[18–22]. Our present study demonstrated that LNP-mediated mRNA delivery effectively edits colonic epithelial cells, enhances efferocytosis in a local tissue environment, and confers therapeutic benefits, providing a convenient and effective strategy for treating inflammatory diseases via efferocytic reprogramming of phagocytes in situ. In our observations, direct intraperitoneal administration of LNPs achieved efficient editing in intestinal epithelial cells, likely attributable to their preferential uptake by phagocytic cells. In contrast, other immune cells in the intestinal tissue, such as T cells, B cells, and macrophages, either exhibited low abundance or minimal editing efficiency, suggesting that epithelial cells serve as the principal mediators of the therapeutic effect. Further studies are needed to optimize the dosing regimen, LNP formulation, and targeting strategies to improve therapeutic outcomes and limit potential toxicities.

Figures

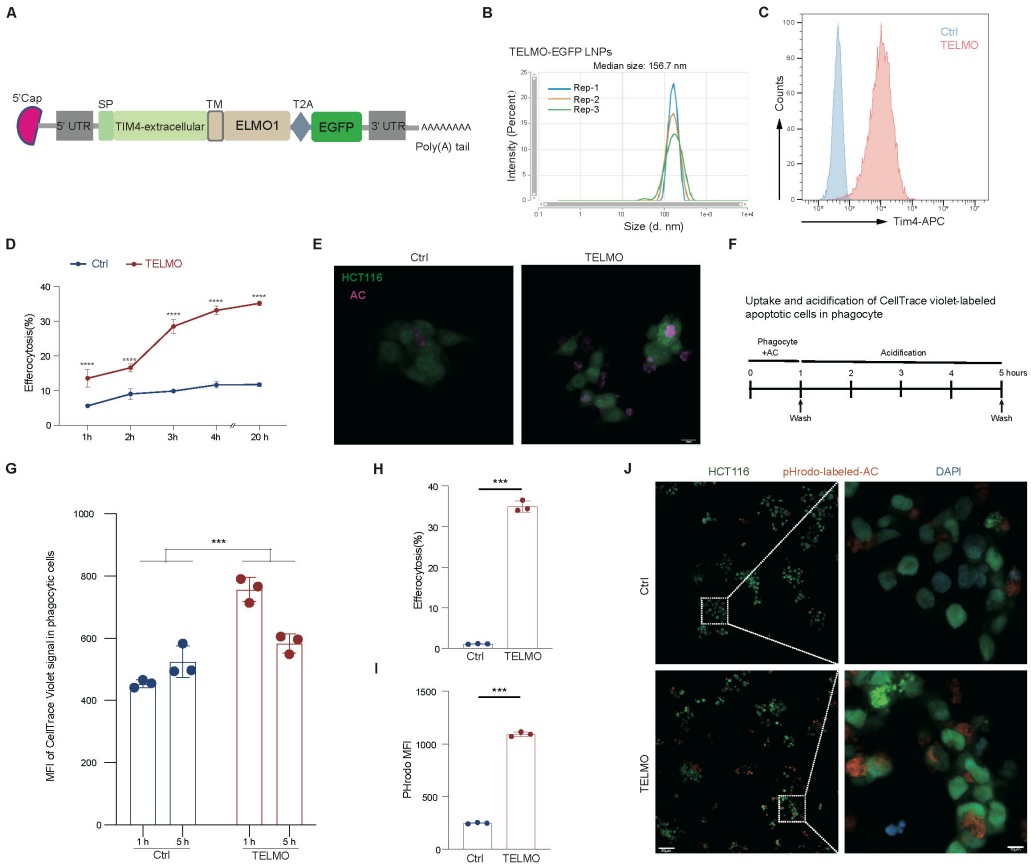

Figure 1. LNP-mediated TELMO expression boosts phagocytosis of apoptotic cells.

(A) Schematic diagram of a TELMO expression construct used for lipid nanoparticle (LNP)-mediated mRNA delivery. SP, signal peptide; TM, transmembrane domain.

(B) Particle diameter distribution of TELMO-EGFP LNPs.

(C) Flow cytometry analysis of TELMO surface expression in HCT116 cells 24 h after TELMO mRNA-LNP transfection.

(D) Quantification of efferocytosis kinetics over time (1-20 hours).

(E) Confocal microscopy images depicting TELMO-expressing HCT116 cells engulfing apoptotic Jurkat cells. Scale bar: 10 μm.

(F) Schematic for the apoptotic corpse acidification assay.

(G) Quantification of acidification levels (MFI reduction) in phagocytosed cargo (n=3).

(H) Quantification of efferocytosis-positive phagocytes.

(I) Quantification of per-cell acidified cargo intensity.

(J) Confocal images confirming apoptotic cell internalization and processing of apoptotic cells.

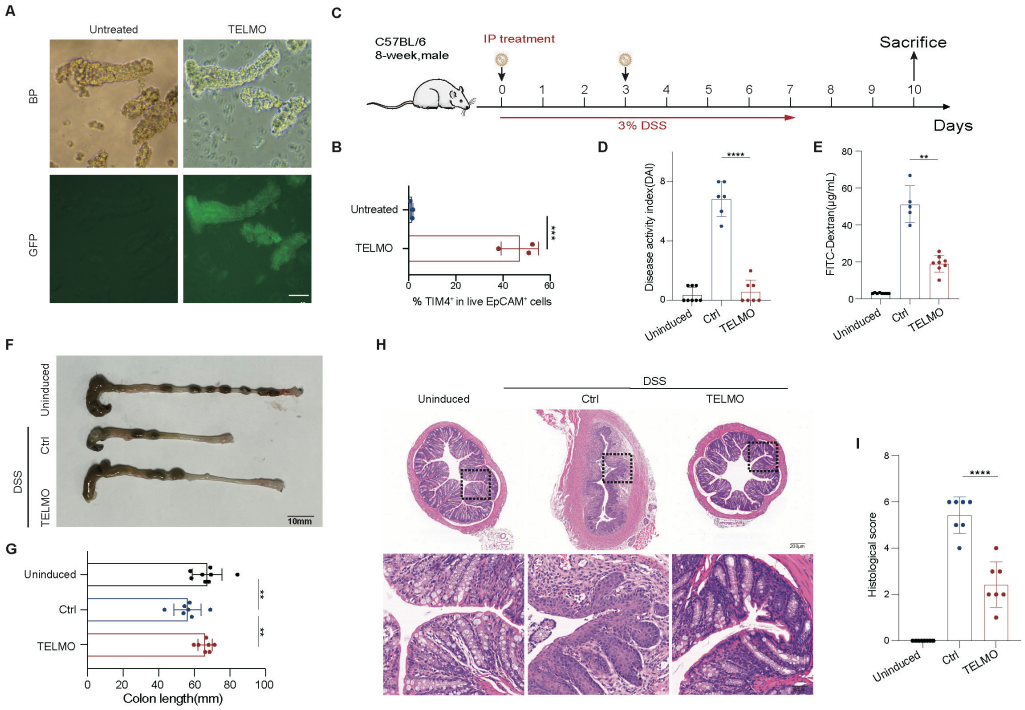

Figure 3. TELMO-LNPs attenuates DSS-induced colitis

(A) Representative fluorescence microscopy images showing GFP expression in colonic epithelial cells 24 hours after intraperitoneal administration of TELMO-GFP LNPs. Both brightfield (BF) and GFP channels are shown for untreated and TELMO-LNP–treated groups. Scale bar: 50 μm.

(B) Quantification of TELMO expression efficiency in EpCAM^{+} colonic epithelial cells(n=3).

(C) Summary of the experimental protocol for DSS-induced colitis model (n=7-10).

(D) Disease activity index (DAI) scores for colitis mice.

(E) Serum FITC–dextran concentration as an index of intestinal permeability.

(F, G) Representative images and quantification of colon length at sacrifice.

(H) Representative Hematoxylin and eosin (H&E) staining of distal colon sections. Scale bars: 200 μm (overview), 50 μm (zoom).

(I) Histologic score derived from the H&E-stained sections.

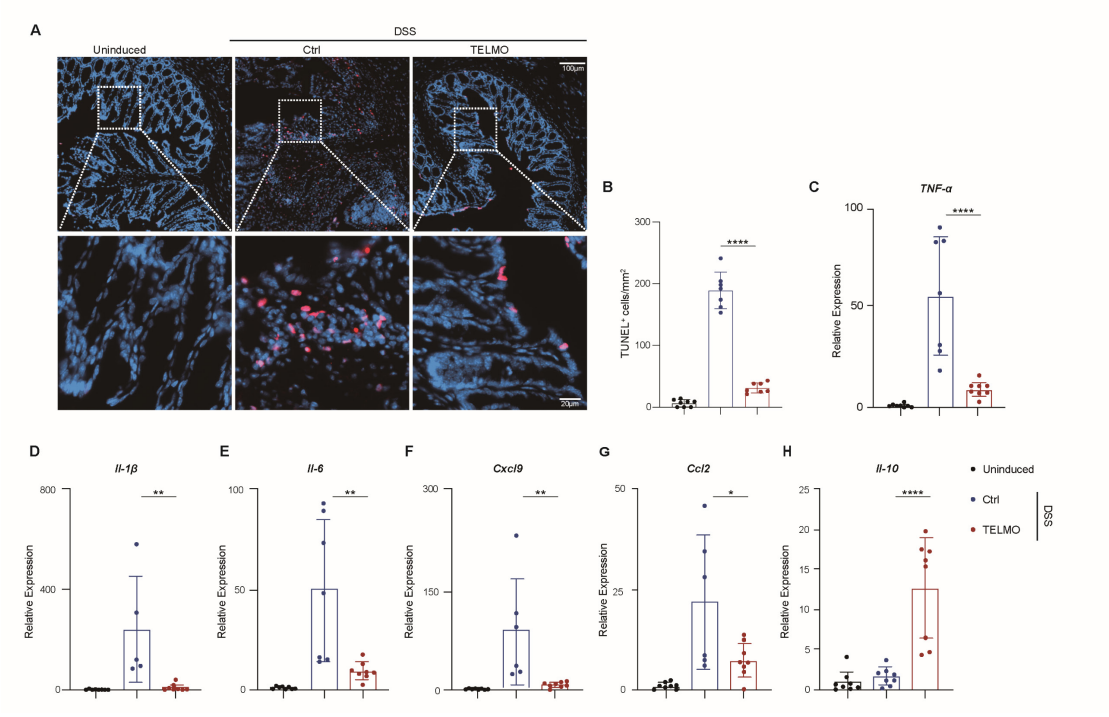

Figure 3. TELMO-LNPs reduce the apoptotic cell burden in tissues and alleviate tissue inflammation.

(A) TUNEL staining of colon sections. 100 μm (overview), 20 μm (zoom).

(B) Quantitative analysis of TUNEL staining.

(C-H) Colonic mRNA expression of pro-inflammatory cytokines (TNF-α, IL-1β, and IL-6), chemokine-related genes (CXCL9 and CCL-2) and the anti-inflammatory gene IL-10. Data are presented as mean (SEM); significance was determined by unpaired Student's two-tailed t-test, one-way ANOVA, or two-way ANOVA according to test requirements, *P<0.05, **P<0.01, ***P<0.001.

Acknowledgements

We thank the Core Facilities of Liangzhu Laboratory. This work was funded by the National Natural Science Youth Foundation of China (No. 82202039).

Author contributions

J.Z, H.L, and H.Z conceived and designed the experiments. H.Z, H.L, and S.Z performed mainly experiments. H.Z, S.Z and Q.W conducted the mRNA and LNPs production. X.K, Z.Y and N.L participated in animal experiments. H.Z, H.L, and J.Z wrote the paper. All authors contributed to the paper and approved its final version.

Conflict of interest

The authors declare no competing interests.

Keywords

mRNA，Lipid nanoparticles，Efferocytosis， Colitis，inflammation

References

1. Green, D. R. The clearance of dead cells by efferocytosis. *Nat. Rev. Mol. Cell Biol.* **21**, (2020).
2. Doran, A. C., Yurdagul, A. & Tabas, I. Efferocytosis in health and disease. *Nat. Rev. Immunol.* **20**, 254–267 (2020).
3. Poon, I. K. H. & Ravichandran, K. S. Targeting Efferocytosis in Inflammaging. *Annu. Rev. Pharmacol. Toxicol.* **64**, 339–357 (2024).
4. Fullerton, J. N. & Gilroy, D. W. Resolution of inflammation: A new therapeutic frontier. *Nat. Rev. Drug Discov.* **15**, 551–567 (2016).
5. Henson, P. M. & Hume, D. A. Apoptotic cell removal in development and tissue homeostasis. *Trends Immunol.* **27**, 244–250 (2006).
6. Henson, P. M. Cell removal: Efferocytosis. *Annu. Rev. Cell Dev. Biol.* **33**, 127–144 (2017).
7. Morioka, S., Maueröder, C. & Ravichandran, K. S. Living on the Edge: Efferocytosis at the Interface of Homeostasis and Pathology. *Immunity* **50**, 1149–1162 (2019).
8. Mahajan, A., Herrmann, M. & Muñoz, L. E. Clearance deficiency and cell death pathways: A model for the pathogenesis of SLE. *Front. Immunol.* **7**, 1–12 (2016).
9. Mũoz, L. E., Lauber, K., Schiller, M., Manfredi, A. A. & Herrmann, M. The role of defective clearance of apoptotic cells in systemic autoimmunity. *Nat. Rev. Rheumatol.* **6**, 280–289 (2010).
10. Mehrotra, P. & Ravichandran, K. S. Drugging the efferocytosis process: concepts and opportunities. *Nat. Rev. Drug Discov.* **21**, (2022).
11. Lee, C. S. *et al.* Boosting Apoptotic Cell Clearance by Colonic Epithelial Cells Attenuates Inflammation In Vivo. *Immunity* **44**, 807–820 (2016).
12. Morioka, S. *et al.* Chimeric efferocytic receptors improve apoptotic cell clearance and alleviate inflammation. *Cell* **185**, 4887-4903.e17 (2022).
13. Wu, M. *et al.* Enhancement of efferocytosis through biased FPR2 signaling attenuates intestinal inflammation . *EMBO Mol. Med.* **15**, 1–22 (2023).
14. Belmokhtar, C. A., Hillion, J. & Ségal-Bendirdjian, E. Staurosporine induces apoptosis through both caspase-dependent and caspase-independent mechanisms. *Oncogene* **20**, 3354–3362 (2001).
15. Mulder, D. J., Noble, A. J., Justinich, C. J. & Duffin, J. M. A tale of two diseases: the history of inflammatory bowel disease. *J. Crohns. Colitis* **8**, 341–348 (2014).
16. Peterson, L. W. & Artis, D. Intestinal epithelial cells: Regulators of barrier function and immune homeostasis. *Nat. Rev. Immunol.* **14**, 141–153 (2014).
17. Sahin, U., Karikó, K. & Türeci, Ö. MRNA-based therapeutics-developing a new class of drugs. *Nat. Rev. Drug Discov.* **13**, 759–780 (2014).
18. Stadler, C. R. *et al.* Elimination of large tumors in mice by mRNA-encoded bispecific antibodies. *Nat. Med.* **23**, 815–817 (2017).
19. Rurik, J. G. *et al.* CAR T cells produced in vivo to treat cardiac injury. *Science (80-.).* **375**, 91–96 (2022).

20. Hunter, T. L. *et al.* In vivo CAR T cell generation to treat cancer and autoimmune disease. *Science (80-.).* **388**, 1311–1317 (2025).
21. Parhiz, H., Atochina-Vasserman, E. N. & Weissman, D. mRNA-based therapeutics: looking beyond COVID-19 vaccines. *Lancet* **403**, 1192–1204 (2024).
22. Razavi, R., Kegel, M., Muscat-Rivera, J., Weissman, D. & Melamed, J. R. Harnessing mRNA-lipid nanoparticles as innovative therapies for autoimmune diseases. *Mol. Ther. Methods Clin. Dev.* **33**, 101566 (2025).

Supplementary information

Materials and methods

Cell culture

The HCT116 cells were cultured in McCoy's 5A medium supplemented with 10% fetal bovine serum (FBS) and 1% penicillin-streptomycin (P/S) solution. Jurkat T cells were maintained in culture using RPMI 1640 supplemented with 10% FBS and 1% P/S. The cells were incubated at 37 °C in a 5% CO2 humidified atmosphere.

RNA Synthesis and Lipid Nanoparticle Encapsulation

The TELMO construct, as previously described[1], consists of the extracellular phosphatidylserine recognition domains of the efferocytic receptor TIM4 and a specific signaling domain of ELMO (Fig. S1). The sequence was cloned into a plasmid encompassing a T7 promoter, 5' and 3' UTR elements, and a poly(A) tail. Modified mRNA was synthesized using in vitro transcription with T7 RNA polymerase. The transcription reaction was assembled in a 20 μL volume containing 1× transcription buffer, 10 mM each of ATP, CTP, GTP, and N1-methylpseudouridine-5'-triphosphate (N1-Me-pUTP), 10 mM 5'-capping analog (CAP GAG 3'OMe), 1 μg template DNA, and T7 RNA polymerase mix. The reaction was incubated at 37°C for 4-8 hours. Template DNA was removed by treatment with RNase-free DNase I at 37°C for 15 minutes. RNA was purified

300 using lithium chloride precipitation. Briefly, the transcription reaction was diluted
301 with 30 μL RNase-free water and 30 μL of 7.5 M LiCl, then precipitated
302 overnight at -20°C. The precipitate was collected by centrifugation at maximum
303 speed for 15 minutes at 4°C, washed with ice-cold 70% ethanol, air-dried, and
304 resuspended in 50 μL RNase-free water to achieve a final concentration of
305 approximately 1 μg/μL. Purified mRNA was stored at -80°C until use. The
306 purified RNA was encapsulated into LNPs by rapidly mixing it with an ethanol
307 lipid mixture containing separable cationic lipids, phospholipids, cholesterol,
308 and PEG-lipid at an acidic pH.

309 **Apoptosis induction and assessment**

310 For induction of apoptosis, human Jurkat T cells, resuspended in RPMI with 1%
311 BSA, were treated with 1 μM staurosporine (STS; MCE) and incubated for 4 h
312 at 37 °C and 5% CO_2. Then apoptotic cells were stained with annexin V-FITC
313 (BioLegend) for 15 min at room temperature in annexin V binding buffer and
314 Propidium Iodide (PI; Yeasen) was added 5 minutes prior to running.

315 **Efferocytosis assay**

316 The target apoptotic cells were stained with CellTrace Violet or pHrodo
317 Red (Thermo Fisher Scientific) before use in the engulfment assays. HCT116
318 cells were plated in a 24-well plate, and co-incubated with targets at a 1:10
319 phagocyte to target ratio for the indicated times. Unbound/unengulfed targets
320 were then washed away with PBS. After the indicated incubation times, cells

321 were harvested for flow cytometric analysis or fixed with DAPI nuclear stain
322 (MCE) for fluorescence microscopy examination.

323 **DSS-induced colitis model**

324 Mice (C57BL6, 8~10 weeks old) received 3% dextran sulfate sodium (DSS; MP
325 Biomedicals) in drinking water for the indicated days, subsequently replaced
326 with regular drinking water until experimental termination. Changes in body
327 weight and disease severity index were monitored daily. Disease severity was
328 quantified using the Disease Activity Index (DAI) scoring system incorporating
329 weight loss, occult blood, and stool consistency, as previously described[2,3]. The
330 total scores were calculated as follows: weight loss（(0: < 1 %, 1: 1~5 %, 2:
331 6~10 %, 3: 11~20 %, 4: > 20 %), stool blood（(0: negative, 1:positive
332 Hemoccult;2: visible blood traces in stool, 3: gross rectal bleeding) , and stool
333 consistency (0: normal;1: semi-formed stools that did not adhere to the anus;2:
334 pasty semi-formed stool that adhered to the anus; 3: liquid stools that adhered
335 to the anus).

336 **Fluorescein isothiocyanate (FITC) labeled dextran permeability assay**

337 Intestinal permeability was assessed through the oral FITC-dextran tracer
338 administration. Mice underwent 4-hour food restriction before intragastric
339 delivery of FITC-labeled dextran (4000 Da, 0.2 mg/g bodyweight, #FD150S;
340 Sigma-Aldrich) suspended in 100 μL phosphate-buffered saline. After 4 h,
341 mouse blood was collected to obtain the hemolysis-free serum for fluorescence
342 intensity detection using the Tecan spark multimode microplate reader

343 (excitation: 488 nm, emission: 520 nm). FITC-dextran serum concentrations
344 were determined against standard dilution curves prepared in PBS buffer.

345 **Histological Analysis**

346 Distal colon segments (0.5 cm from anus) were fixed, paraffin-embedded, and
347 sectioned (4 μm) for hematoxylin and eosin (H&E) staining. Histological scores
348 of colitis were assessed based on an established scoring criteria.[3] Briefly,
349 inflammation severity was scored as: 0, normal (within normal limits); 1, mild
350 (focal inflammation limited to lamina propria); 2, moderate (multifocal or locally
351 extensive inflammation extending to submucosa); 3, severe (transmural
352 inflammation with ulcers affecting >20 crypts). Ulceration was scored as: 0,
353 normal (no ulcers); 1, mild (1-2 ulcers affecting ≤20 crypts); 2, moderate (3-4
354 ulcers affecting 20-40 crypts); 3, severe (>4 ulcers or >40 crypts affected).
355 Apoptotic cell detection was performed using TUNEL methodology following
356 manufacturer's protocol (YSFluorTM 640; Yeasen).

357 **Quantitative RT-PCR**

358 Total RNA from the colons extracted using the FastPure Complex Tissue/Cell
359 Total RNA Isolation Kit (Vazyme). Then, cDNA was generated using the
360 EasyScript One-Step gDNA Removal and cDNA Synthesis SuperMix kit
361 (TransGen Biotech). Quantitative PCR was then performed with a ChamQ Blue
362 Universal SYBR qPCR Master Mix Kit (Vazyme) to profile the gene expressions,
363 using histone gene *Gapdh* as the standard control. All qPCR primers (5′→3′)
364 were designed using Primer-BLAST (NCBI) and validated experimentally.

365 Primer sequences are provided in Supplementary Table1.

366

367

368 ## References

369 1 Morioka, S. et al. Chimeric efferocytic receptors improve apoptotic cell clearance and alleviate
370 inflammation. Cell 185, 4887-4903.e4817, doi:10.1016/j.cell.2022.11.029 (2022).
371 2 Sun, D. et al. Angiogenin maintains gut microbe homeostasis by balancing α-Proteobacteria
372 and Lachnospiraceae. Gut 70, 666-676, doi:10.1136/gutjnl-2019-320135 (2021).
373 3 Zaki, M. H. et al. The NOD-like receptor NLRP12 attenuates colon inflammation and
374 tumorigenesis. Cancer Cell 20, 649-660, doi:10.1016/j.ccr.2011.10.022 (2011).
375

Supplementary figures

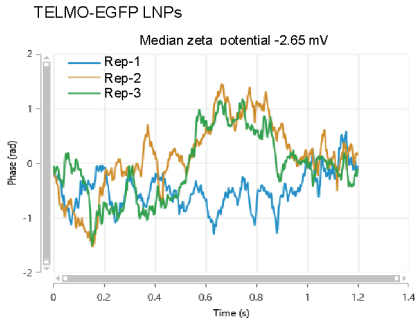

Supplementary Figure S1. Zeta potentials of TELMO-EGFP LNPs

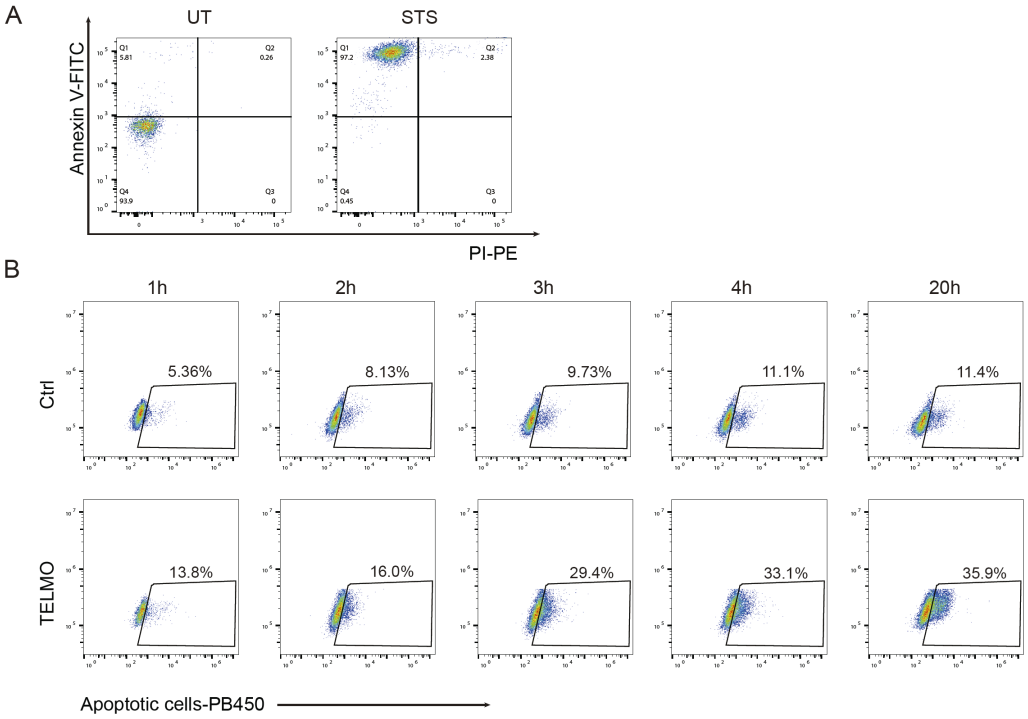

Supplementary Figure S2. Apoptosis validation and time-course analysis of apoptotic cell uptake by TELMO-expressing cells.

(A) Flow cytometric analysis of early apoptotic Jurkat cells following 4-hour staurosporine (STS) treatment, detected by Annexin V and propidium iodide (PI) double staining.

385 (B) Representative flow cytometry plots showing uptake of CellTrace Violet–labeled

386 apoptotic Jurkat cells by TELMO-expressing HCT116 cells over 1–20 h co-culture(n=3).

387

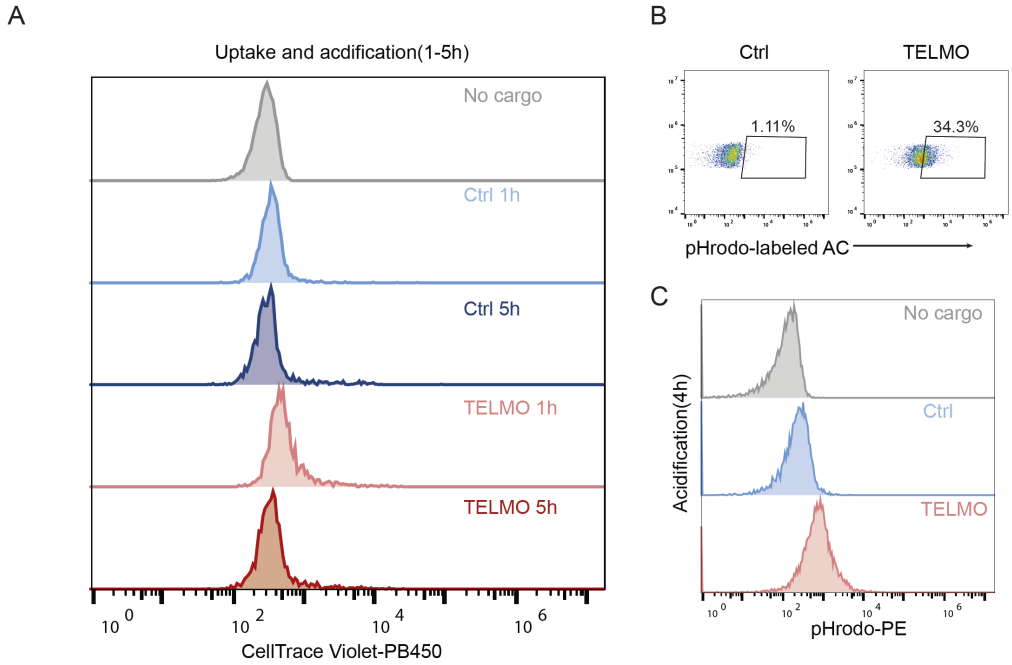

388

389 **Supplementary Figure S3. Phagolysosomal acidification in TELMO**

390 **phagocytes.**

391 (A) Flow cytometry analysis of acidification levels in phagocytosed cargo,

392 measured as mean fluorescence intensity (MFI) reduction.

393 (B, C) Flow cytometry evaluation of acidic compartment trafficking using a pH-

394 sensitive reporter dye: proportion of pHrodo^{+} phagocytes (B) and per-cell cargo

395 intensity (C) (n=3).

396

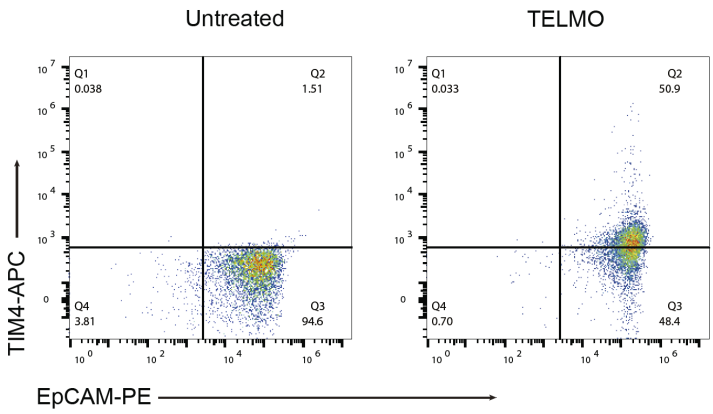

Supplementary Fig. S4. TELMO-LNP delivery to colonic epithelial cells.

Flow cytometry plots showing TELMO expression in EpCAM⁺ colonic epithelial cells following intraperitoneal TELMO-LNP administration(n=3).

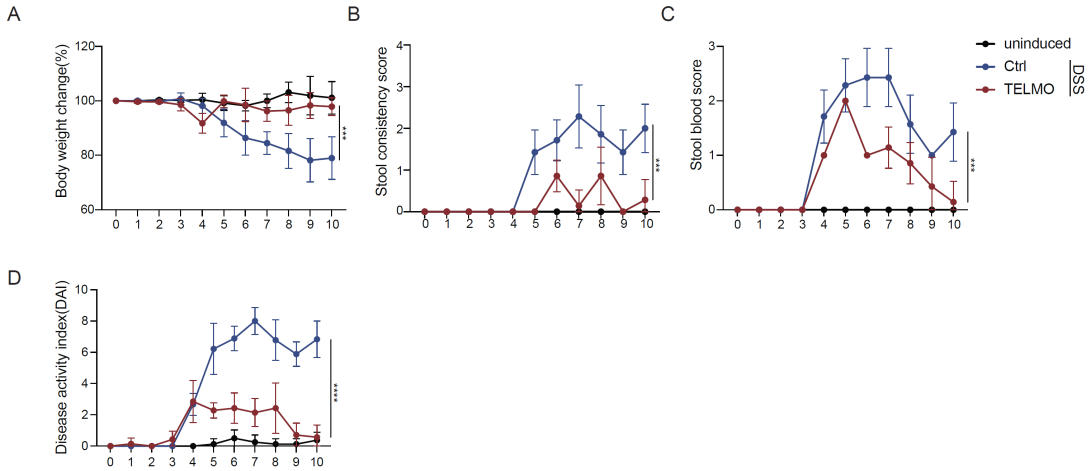

Supplementary Fig. S5. Therapeutic efficacy of TELMO-LNP treatment in DSS-induced colitis.

Clinical assessment of dextran sulfate sodium (DSS)-induced colitis in vehicle-treated control and TELMO-LNP–treated mice (n = 7–8 mice per group). Parameters include: body weight change from baseline(A), stool consistency score (B), rectal bleeding score (C), and (D) composite Disease Activity Index (DAI) calculated from the sum of individual clinical scores. Data represent mean

± SEM; significance was determined by two-way ANOVA, ***p < 0.001, ***p < 0.0001.

Gene	Primer Sequence (5′→3′)	Direction
GAPDH	AGGTCGGTGTGAACGGATTTG	Forward (F)
GAPDH	TGTAGACCATGTAGTTGAGGTCA	Reverse (R)
IL6	CCAAGAGGTGAGTGCTTCCC	Forward (F)
IL6	CTGTTGTTCAGACTCTCTCCCT	Reverse (R)
TNFα	CCCTCACACTCAGATCATCTTCT	Forward (F)
TNFα	GCTACGACGTGGGCTACAG	Reverse (R)
IL1β	TGCCACCTTTTGACAGTGATG	Forward (F)
IL1β	ATGTGCTGCTGCGAGATTTG	Reverse (R)
IL10	GGCCCAGAAATCAAGGAGCA	Forward (F)
IL10	AGACACCTTGGTCTTGGAGCTTAT	Reverse (R)
CXCL9	TCCTTTTGGGCATCATCTTCC	Forward (F)
CXCL9	TTTGTAGTGGATCGTGCCTCG	Reverse (R)
MCP1	CAGATGCAGTTAACGCCCCA	Forward (F)
MCP1	TGAGCTTGGTGACAAAAACTACAG	Reverse (R)

Supplementary Table 1. List of primers used for quantitative real-time PCR (qPCR).